JOURNAL OF GEOPHYSICAL RESEARCH, VOL. 107, NO. B3, 2046, 10.1029/2001JB000268, 2002

# Fabric of the Rio Ceará–Mirim mafic dike swarm (northeastern Brazil) determined by anisotropy of magnetic susceptibility and image analysis

Carlos J. Archanjo and Marcelus G. S. Araújo
Instituto de Geociências, Universidade de São Paulo, São Paulo, Brazil

Patrick Launeau
Laboratoire de Planétologie et Géodynamique, Faculté de Sciences et des Techniques, Université de Nantes, Nantes, France

Received 1 September 2000; revised 23 May 2001; accepted 25 September 2001; published 7 March 2002

[1] Anisotropy of magnetic susceptibility (AMS) and petrofabric studies of the Early Cretaceous Rio Ceará–Mirim dike swarm reveal that shape-preferred orientation of opaque grains controls the magnetic fabric. The 350-km-long swarm is characterized by relatively thick dikes, of the order of 20 m up to 150 m in width. The strong magnetic susceptibility of these rocks, around $5 \times 10^{-2}$ SI, is attributed to magnetite with low Ti content. The magnetite usually forms euhedral to subhedral, equant to skeletal grains. The resulting AMS has a large proportion of abnormal fabric types, as observed in 58% of the 50 dikes studied. The remaining 42% of the dikes show a "normal" fabric regionally characterized by steep magnetic foliations and subhorizontal lineations. In the central eastern part of the swarm, however, the lineation plunges downdip, suggesting a magmatic feeder zone. The shape alignment of the plagioclase supports the inferred regional flow pattern, indicating a primary origin for the normal AMS. Inverse to highly imbricate magnetic fabrics have lineations perpendicular to, or at a high angle to, the dike wall. A shape lineation of opaque grains lies generally close to the magnetic lineation, while the foliation is provided by the oblate-shaped plagioclase fabric. Petrofabric studies indicate that the abnormal magnetic fabric is unrelated to flow. Competition of interstitial magnetite grains crystallizing either along, as well as perpendicular to the magma stretching direction seems to account for the weak magnetic anisotropy and the irregular distribution of the AMS types on the swarm. *INDEX TERMS:* 1518 Geomagnetism and Paleomagnetism: Magnetic fabrics and anisotropy; 8025 Structural Geology: Mesoscopic fabrics; 9360 Information Related to Geographic Region: South America; 9609 Information Related to Geologic Time: Mesozoic; *KEYWORDS:* magnetic fabric and anisotropy, mesoscopic, Fabrics, South American, Mesozoic

## 1. Introduction

[2] Anisotropy of magnetic susceptibility (AMS) has been able to reveal the subtle alignment of mineral grains, even for visually isotropic rocks such as mafic dikes [*Knight and Walker*, 1988]. A usual model is that the shape-preferred orientation of Ti-magnetite mimics the geometry of flow within the dike; that is, the maximum susceptibility ($k_1$) is subparallel to the flow direction and the minimum susceptibility ($k_3$; $k_1 \geq k_2 \geq k_3$) is perpendicular to the confining wall. This "normal magnetic fabric" has been observed in basalt containing multidomain (MD) and/or pseudosingle-domain magnetite grains. The concordance of the maximum susceptibility direction (magnetic lineation $k_1$) and outcrop flow indicators (elongate vesicles, trachitic fabric, and "hot slickenlines") [*Knight and Walker*, 1988; *Varga et al.*, 1998] has encouraged the use of AMS in the study of the emplacement of mafic dike swarms in different geodynamic settings [e.g., *Ernst*, 1990; *Rochette et al.*, 1991; *Ernst and Baragar*, 1992; *Raposo and Ernesto*, 1995; *Varga et al.*, 1998; *Archanjo et al.*, 2000].

[3] However, normal magnetic fabrics are not the only fabric types observed in dikes. In the Oman [*Rochette et al.*, 1991] and Ponta Grossa [*Raposo and Ernesto*, 1995] swarms, for example, only 50% of the dikes show normal fabrics. The remaining "abnormal" magnetic fabrics show inverse ($k_1$ and $k_3$ axes and symmetry are inverted) or intermediate fabrics ($k_1$ and $k_2$ or $k_2$ and $k_3$ are exchanged). Departure from normal magnetic fabric has usually been interpreted as evidence for (1) a secondary, post-emplacement modification of the fabric by cooling or tectonic stresses [*Elwood*, 1978; *Park et al.*, 1988], (2) the occurrence of fine-grained, single-domain (SD) magnetite which has an inherently inverse fabric [*Stephenson et al.*, 1986], or (3) a primary feature-related particle flow, which rotated freely in a viscous fluid [*Dragoni et al.*, 1997]. In the latter, the cause of the abnormal fabrics could be the "rolling" of elongate particles in a flow field [*Jeffery*, 1922]. Models using an assembly of rigid ellipsoidal grains of magnetite rotating in a viscous fluid were able to develop intermediate to oblique-type fabrics [*Dragoni et al.*, 1997]. So, many abnormal magnetic fabrics could have a primary origin principally because rock magnetic studies in mafic dikes were not able to detect SD particles [*Rochette et al.*, 1992; *Tauxe et al.*, 1998]. Because the contention about the origin and meaning of inverse or intermediate-type magnetic fabrics [*Rochette et al.*, 1999], a sample strategy to reduce the occurrence of such "undesirable" fabrics was proposed by *Tauxe et al.* [1998]. It consists in coring some 10 cm of dike margin to avoid flow complications (e.g., back flow [*Philpotts and Asher*, 1994]), particularly in long-lived thick dikes [*Fialko and Rubin*, 1999]. This strategy applied to the Troodos Ophiolite clearly improved the quality of the AMS


0148-0227/02/2001JB000268$09.00

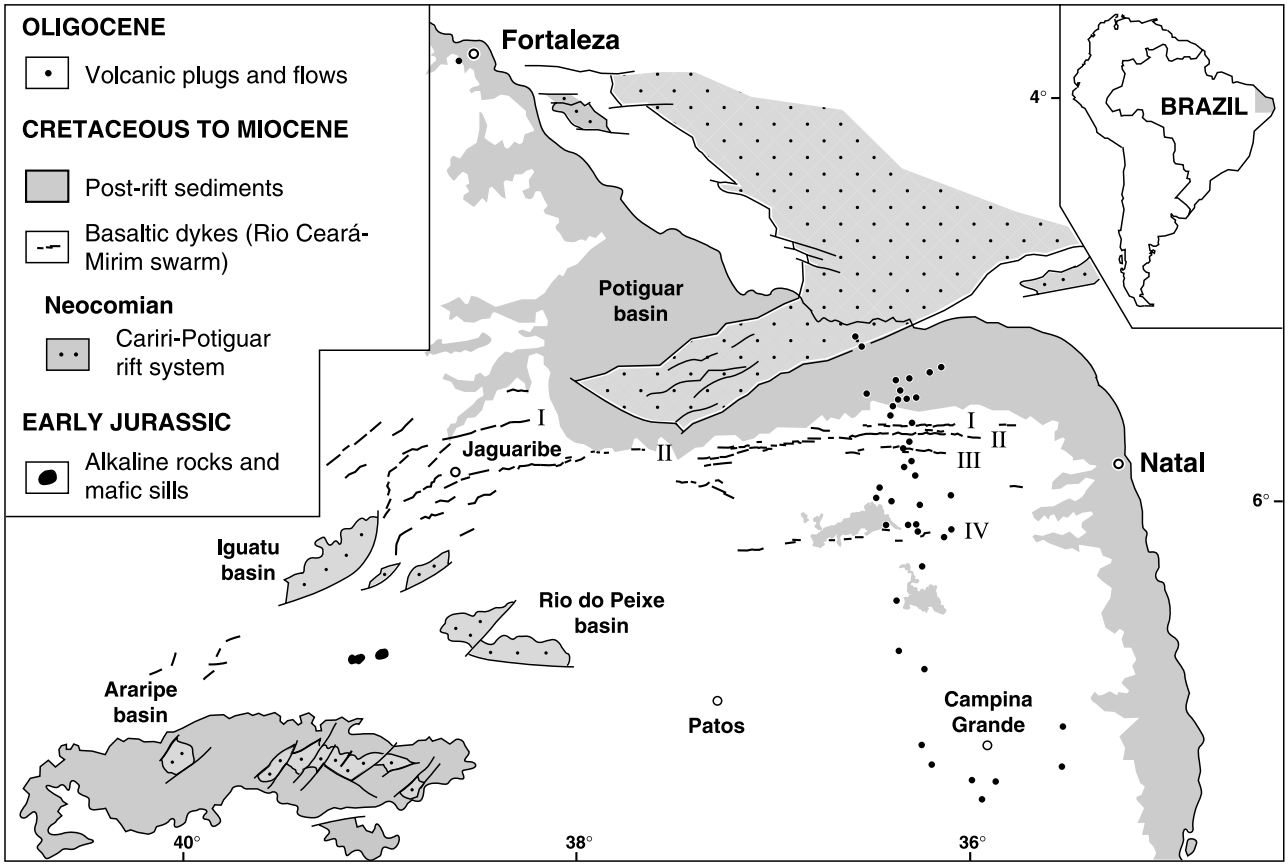


**Figure 1.** Sketch map showing the distribution of the basaltic rocks of northeastern Brazil, specifically the Mesozoic Rio Ceará–Mirim Dike Swarm and Tertiary volcanic plugs and lava flows. Subswarms I–IV are labeled after *Bellieni* [1992] and the position of onshore/offshore Cariri-Potiguar Rift System is after *Matos* [1992].

data and permitted the use of imbricate fabrics near the dike margins to fix the flow sense [*Varga et al.*, 1998].

[4] This paper presents a combination of AMS and image analysis of the 350-km-long, Rio Ceará–Mirim Dike Swarm (CMDS) of northeastern Brazil (Figure 1). This swarm represents a precursor of the opening of the equatorial Atlantic and could be related to the Santa Helena hot spot, according to the inferred location of this hot spot at 130–120 Ma [*Morgan*, 1983; *O'Connor and Le Roex*, 1992]. A paleomagnetic study on the CMDS showed different magnetization directions from one dike set to another, which led *Bellieni* [1992] to group the dikes into four subswarms (I–IV in Figures 1 and 2). Our study deals with subswarms I, II,

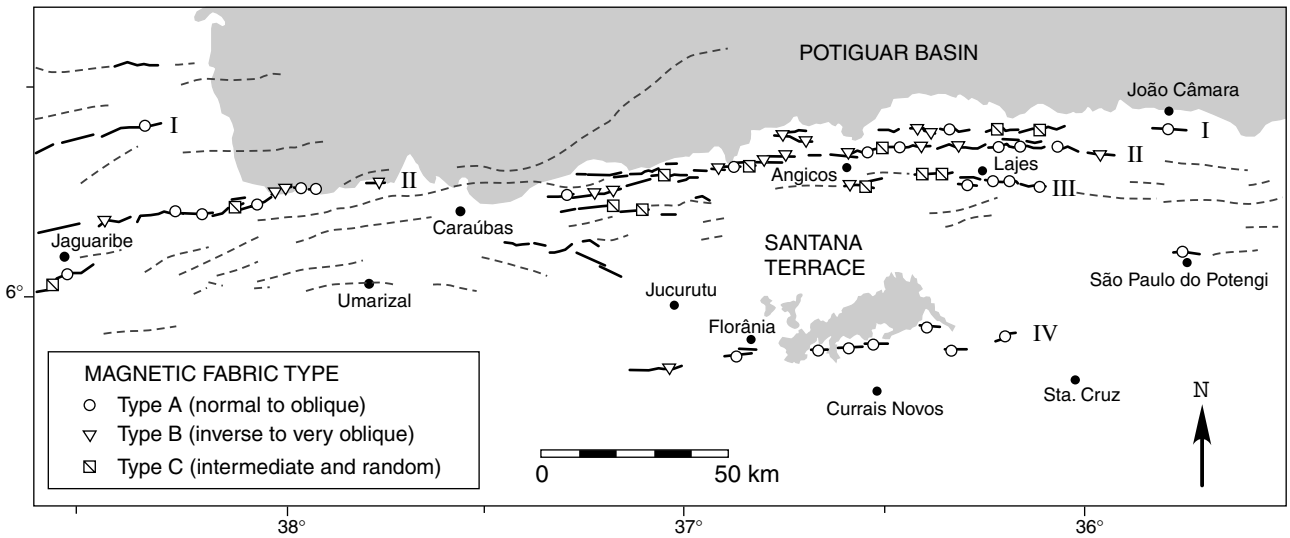


**Figure 2.** Magnetic fabric types of the Rio Ceará–Mirim subswarms I, II, III, and IV. Dashed thinnest lines are the aeromagnetic anomalies attributed to mafic dikes [after *Oliveira*, 1992].

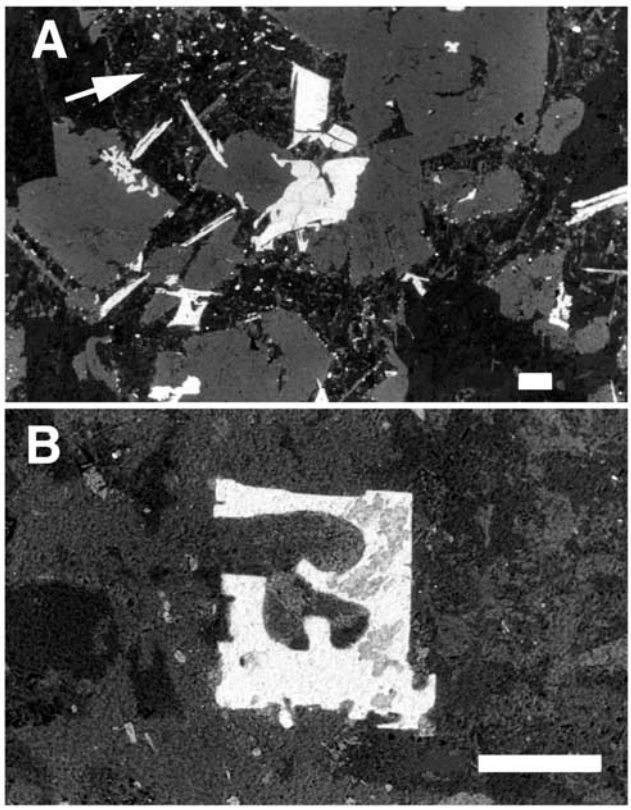


**Figure 3.** Backscattered electron images of the textural features of oxide and silicate grains. (a) ''Primary'' euhedral to subhedral oxide grains, some of which show skeletal and elongated (rod-like) morphologies. Fine oxide grains occur around the silicates and dispersed in the altered matrix (arrow). (b) Magnetite crystal preserving embayed contacts with the silicate matrix. Scale bar is 100 μm long.

and III (see *Archanjo et al.* [2000] for subwarm IV). Some 42% of the 50 dikes sampled show normal magnetic fabrics, 34% are inverse to very oblique, and 24% show fabric types that cannot be interpreted (Figure 2). The structural significance of these magnetic fabrics was compared with the shape-preferred orientation (SPOs) of plagioclase and opaque grains by determining the tensor inertia of mineral phases in digital images of thin sections [*Launeau and Cruden*, 1998]. This method determines the average subfabric of each classified mineral phase and is therefore appropriate for comparison with the AMS, which measures the bulk magnetic fabric of the rock.

## 2. Geological Setting

[5] The Rio Ceará–Mirim Dike Swarm cuts the structural grain of the Precambrian basement at a high angle, intruding a set of fractures trending E-W at the southern edge of the onshore region of the Potiguar Basin (Figure 1). In the western part of the swarm these dikes become nearly parallel to the NE-SW trending Cariri-Potiguar Rift System. Individual dikes crop out as vertical bodies <1 km long and 1.2 m up to 150 m wide. Dikes 20–100 m wide are relatively common. A few sets form an en echelon pattern indicating that the emplacement occurred at a high crustal level. The available aeromagnetic data [*Oliveira*, 1992] show that magnetic anomalies attributed to mafic dikes generally occur as closely spaced strips some 10–40 km long with amplitudes that vary from 50 to 300 nT (Figure 2). In the western part of the swarm, there occur a few dikes the length of which exceeds 100 km. The arcuate trajectory of the CMDS is suggestive of a change in the minimum stress axis from NW-SE in the western part of the swarm to N-S in the central and eastern parts [*Oliveira*, 1992]. This is consistent with the NE-SW oriented intracontinental Potiguar-Cariri rift basin, formed by the reactivation of ancient zones of crustal weakness during the initial extensional event related to the opening of the equatorial Atlantic [*Matos*, 1992].

[6] The basaltic magmatism is tholeiitic in composition, being derived from a large-ion lithophile (LIL) enriched mantle source [*Bellieni*, 1992]. It shows K-Ar ages ranging between 145 and 120 Ma (Neocomian to Aptian), with two peaks of activity at 140 and 130 Ma [*Oliveira*, 1992]. The CMDS is contemporaneous with basalt and rhyolithic flows of the northern Benue Trough in Nigeria [*Maluski et al.*, 1995]. In Tertiary times, basaltic plugs and lava flows erupted in northeastern Brazil forming a volcanic chain trending N-S (Figure 1). The plugs have elliptical to subcircular shapes with maximum diameter of 200 m and cross the CMDS in the eastern part of the Santana Terrace and around Lajes. The lava flows of the Tertiary suite consist of olivine basalt, whereas the plugs are composed of olivine nephelinite and basanite [*Sial et al.*, 1981].

## 3. Petrography and Oxide Textures

[7] The dikes generally display typical onionskin weathering, forming centimetric to metric oval-shaped blocks settled in a dark argillaceous soil. In the center of the blocks the rock is fresh, consisting of medium- to fine-grained basalt. In thin section the crystals occur as a mosaic of euhedral to subhedral labradorite, augite, pigeonite, and opaque grains. Titanomagnetite is the main opaque mineral [*Bellieni*, 1992], and olivine is found as an accessory mineral in some dikes of subswarm IV.

[8] The dikes exhibit a range of textures from subophitic to seriate to intergranular, with clinopyroxene commonly forming large 0.3–2.0 mm equant grains. Plagioclase laths, 0.4–2.5 mm long, are partially enclosed in clinopyroxene or form an intergranular texture with clinopyroxene and opaque occupying the spaces between them. In thin section, cryptocrystalline material is normally observed in variable amounts, and it appears to be associated with the chemical alteration of clinopyroxene and calcic plagioclase. Thin section and backscattered electron examination of this fine-grained material revealed the presence of calcite and minute magnetite particles, the latter also observed included within crystals of clinopyroxene and plagioclase (Figure 3a). The Fe-Ti oxides occur as two textural types [*Archanjo et al.*, 2000]: (1) euhedral to subhedral crystals (mean grain size of 100 μm) containing minute inclusion of silicates and (2) needle-like crystals up to 500 μm long and 2–8 μm wide, some showing skeletal growth morphologies (Figure 3a). Among the oxide grains, titanomagnetite is quite abundant (2.5–6% by volume) and may be present in crystals up to 2 mm. Ilmenite is comparatively scarce and occurs as small elongated laths [*Bellieni*, 1992]. A close examination of the textural relationships between silicates and Fe-Ti oxides shows that the contacts vary from sharp to irregular, locally cuspate. Most oxide grains have embayed contacts with the silicate matrix suggestive of subsolidus reactions (Figure 3b). These reactions seem to have occurred by high-temperature oxidation during cooling stages, as indicated by the occurrence of fine ilmenite exsolution lamellae within magnetite [*Bucker et al.*, 1986].

## 4. Anisotropy of Magnetic Susceptibility Study

### 4.1. Sampling and Analytical Methods

[9] The samples of the 49 dikes were obtained from the largest rock blocks found, apparently in place and as fresh as possible. In three cases where it was possible to sample the wall rock contact,

**Table 1.** Site-Mean Anisotropy of Magnetic Susceptibility of the Rio Ceará–Mirim Dikes[a]

| Site | Localization (UTM Coordinate) | Scalar Data | | | Directional Data | | | | Fabric Type | Observations |
|---|---|---|---|---|---|---|---|---|---|---|
| | | Km, $10^{-2}$ SI | $P$ | $T$ | $K_1$ | $K_2$ | $K_3$ | $a_1/a_3$ | | |
| 1 | 805.64/9368.08 | 8.981 | 1.025 | −0.122 | 111,70 | 284,22 | 011,02 | 20/28 | A | $w$ = 90 m |
| 2 | 810.69/9367.38 | 7.321 | 1.017 | −0.501 | 170,74 | 283,06 | 014,16 | 06/22 | A | $w$ = 65 m |
| 3 | 171.05/9373.85 | 5.282 | 1.014 | 0.613 | 158,24 | 243,03 | 342,60 | 40/13 | B | |
| 4 | 818.65/9366.38 | 10.488 | 1.016 | 0.150 | 105,31 | 305,58 | 201,13 | 21/16 | A | |
| 5 | 786.91/9369.36 | 6.706 | 1.010 | −0.111 | 222,33 | 011,57 | 130,09 | 32/34 | R | $w$ = 70 m |
| 6 | 766.34/9374.27 | 7.858 | 1.020 | 0.329 | 013,02 | 283,02 | 122,88 | 19/07 | B | |
| 7 | 778.67/9376.67 | 4.580 | 1.027 | 0.724 | 272,16 | 022,50 | 172,35 | 21/08 | A | |
| 8 | 795.21/9376.95 | 4.697 | 1.010 | 0.368 | 237,26 | 344,30 | 113,47 | 20/09 | *R | |
| 9 | 792.80/9382.02 | 4.943 | 1.030 | 0.294 | 080,22 | 216,59 | 343,18 | 11/12 | A | $w$ = 60 m |
| 10 | 810.58/9376.66 | 4.635 | 1.023 | 0.525 | 350,83 | 087,06 | 183,12 | 32/15 | A | |
| 11 | 820.86/9381.74 | 6.502 | 1.018 | −0.150 | 036,14 | 154,52 | 305,43 | 29/31 | R | $w$ = 130 m |
| 12 | 193.75/9376.79 | 6.857 | 1.014 | 0.0000 | 282,07 | 022,78 | 184,08 | 22/29 | A | |
| 13 | 821.43/9376.92 | 5.250 | 1.009 | 0.277 | 273,09 | 026,58 | 173,33 | 27/22 | A | |
| 14 | 806.99/9376.66 | 7.291 | 1.051 | 0.000 | 276,80 | 133,08 | 040,09 | 24/22 | A | |
| 15 | 767.95/9369.15 | 3.723 | 1.008 | −0.493 | 047,01 | 143,46 | 310,21 | 27/41 | R | |
| 16 | 790.68/9381.26 | 7.995 | 1.005 | −0.659 | 014,40 | 273,10 | 192,46 | 20/38 | B | |
| 17 | 794.40/9370.00 | 9.201 | 1.010 | 0.258 | 108,09 | 024,33 | 203,61 | 34/24 | *R | |
| 18 | 787.87/9382.34 | 4.929 | 1.068 | 0.818 | 207,17 | 114,11 | 345,72 | 29/09 | B | |
| 19 | 788.13/9377.66 | 4.617 | 1.005 | −0.773 | 191,21 | 287,13 | 062,70 | 20/36 | B | |
| 20 | 767.95/9369.15 | 4.142 | 1.012 | −0.823 | 046,29 | 165,48 | 303,33 | 29/29 | *R | |
| 21 | 579.39/9357.85 | 5.475 | 1.010 | −0.204 | 084,43 | 216,35 | 326,27 | 08/18 | A | |
| 22 | 767.95/9369.15 | 7.595 | 1.015 | −0.055 | 168,01 | 232,32 | 017,79 | 36/31 | B | $w$ = 30 m |
| 23 | 741.88/9372.93 | 6.741 | 1.004 | 0.609 | 278,11 | 183,04 | 014,37 | 40/33 | R | |
| 24 | 737.83/9372.58 | 4.943 | 1.015 | 0.268 | 274,79 | 101,12 | 011,04 | 17/13 | A | |
| 25 | 769.26/9374.66 | 11.750 | 1.007 | 0.239 | 114,03 | 025,17 | 233,81 | 38/20 | R | |
| 27 | 723.43/9368.75 | 3.148 | 1.015 | 0.285 | 208,16 | 115,09 | 351,75 | 20/13 | B | |
| 28a | 804.95/9368.26 | 2.499 | 1.042 | 0.000 | 119,69 | 271,21 | 003,11 | 14/18 | A | $w$ = 1.5 m |
| 28b | | 2.542 | 1.038 | 0.179 | 072,65 | 259,27 | 168,03 | 10/18 | A | |
| 28c | | 3.349 | 1.018 | 0.304 | 082,52 | 226,30 | 319,18 | 26/21 | A | |
| 29 | 716.70/9368.63 | 5.608 | 1.007 | 0.410 | 216,53 | 324,02 | 068,32 | 35/25 | R | |
| 30a | 743.80/9374.70 | 4.249 | 1.017 | 0.184 | 191,01 | 281,32 | 095,58 | 17/14 | B | $w$ = 18 m |
| 30c | | 5.126 | 1.010 | −0.779 | 215,11 | 313,20 | 121,75 | 16/32 | B | |
| 31 | 749.50/9374.50 | 7.746 | 1.021 | 0.139 | 153,14 | 048,45 | 256,41 | 10/07 | B | |
| 32 | 710.20/9361.50 | 6.544 | 1.007 | −0.075 | 090.15 | 152.10 | 022,41 | 32/35 | R | |
| 33 | 705.47/9366.07 | 8.389 | 1.014 | 0.000 | 215,12 | 314,15 | 098,70 | 22/24 | B | |
| 34 | 708.99/9367.47 | 4.137 | 1.017 | 0.517 | 267,03 | 010,77 | 176,12 | 19/06 | A | |
| 35 | 707.44/9361.26 | 7.779 | 1.016 | −0.252 | 297,19 | 202,24 | 065,58 | 13/25 | *R | |
| 36 | 695.90/9363.80 | 6.128 | 1.017 | −0.601 | 215,06 | 122,28 | 319,61 | 05/21 | B | |
| 37 | 688.89/9362.94 | 4.930 | 1.033 | 0.699 | 267,09 | 038,76 | 177,05 | 29/13 | A | |
| 38a | 636.23/9359.13 | 6.156 | 1.011 | 0.302 | 003,26 | 227,54 | 110,10 | 31/19 | B | $w$ = 25 m |
| 38c | | 5.169 | 1.012 | −0.165 | 157,17 | 077,13 | 326,63 | 32/29 | R | |
| 39 | 606.75/9362.13 | 5.138 | 1.003 | 0.974 | 288,02 | 192,77 | 020,12 | 24/24 | A | $w$ = 40 m; strike 105 Az |
| 40 | 615.66/9360.87 | 4.523 | 1.006 | 0.513 | 135,52 | 285,27 | 023,25 | 28/22 | A | strike 080 Az |
| 41 | 604.18/9363.19 | 3.852 | 1.006 | 0.395 | 167,08 | 258,11 | 050,77 | 17/14 | B | $w$ = 40 m; strike 105 Az |
| 42 | 599.42/9361.37 | 4.820 | 1.009 | 0.186 | 310,04 | 218,14 | 062,74 | 16/20 | B | $w$ = 40 m; strike 070 Az |
| 43 | 594.66/9360.21 | 4.922 | 1.015 | 0.316 | 269,27 | 049,57 | 168,19 | 25/09 | A | $w$ = 170 m |
| 44 | 585.18/9359.81 | 5.847 | 1.007 | 0.178 | 072,15 | 182,58 | 305,31 | 36/34 | R | $w$ = 100 m |
| 45 | 576.48/9358.01 | 4.580 | 1.027 | 0.724 | 272,16 | 022,50 | 172,50 | 21/08 | A | $w$ = 250 m; strike 100 Az |
| 46 | 579.39/9357.86 | 5.753 | 1.018 | 0.732 | 087,13 | 272,80 | 177,08 | 29/22 | B | |
| 47 | 571.30/9356.36 | 4.473 | 1.017 | 0.088 | 018,07 | 168,80 | 287,03 | 18/16 | B | |
| 48 | 576.10/9381.00 | 6.014 | 1.053 | 0.823 | 074,28 | 227,58 | 341,12 | 22/10 | A | |
| 49 | 509.83/9314.06 | 3.782 | 1.005 | −0.712 | 075,61 | 007,11 | 249,37 | 34/42 | R | |
| 50 | 541.01/9340.02 | 5.188 | 1.019 | −0.142 | 221,18 | 065,66 | 316,05 | 17/27 | A | $w$ = 60m; strike 060 Az |

[a] Km, site mean bulk susceptibility; $P$, degree of anisotrophy; $T$, AMS ellipsoid shape parameter [*Jelinek*, 1981]; $K_1$, $K_2$, and $K_3$, site-mean declination (azimuth) and inclination (measured in degrees) of the principal susceptibility directions; $a_1/a_3$, semiangle (measured in degrees) of the long and short axes of the confidence ellipse ($1\sigma$) about site-mean of respective $k_1$ and $k_3$ axes; *R is an intermediate-type AMS fabric (see text); $w$ is dike width; Az is azimuth.

cores were collected at the margin as well as from the central part of the dike. Because of the degree of physical weathering of the dikes (most of them occurring as oval-shaped blocks resulting from spheroidal weathering) it was impossible to use the sample strategy suggested by *Tauxe et al.* [1998]. Four to six oriented cores 2.5 cm in diameter and 6 to 10 cm long were collected at each site using a portable gasoline-powered rock drill. The core spacing at each site varied from a meter up to a few tens of meters. Resampling the same block of basalt was avoided in order to minimize the potential problem of taking cores from blocks not in situ. In the laboratory, each core was cut into 2.2-cm-long specimens, so that each measurement site yielded 8–16 oriented specimens.

[10] Low-field ($3.8 \times 10^{-4}$ T; 920 Hz) anisotropy of susceptibility was measured using the KLY 3S Kappabridge instrument of the Laboratório de Anisotropias Magnéticas of the Instituto de Geociências of the Universidade de São Paulo. The mean susceptibility and the mean orientation of the site are given by the mean tensor of all samples collected at the site; $k_1$ is the mean magnetic lineation, and $k_3$ is the pole of the mean magnetic foliation. The symmetry of the magnetic fabric is represented by the $T$ parameter

**Table 2.** Comparative Bulk Susceptibilities of the Rio Ceará–Mirim Dikes

| | | Km, $10^{-2}$ SI | |
|---|---|---|---|
| Description | $n$[a] | Mean | SD |
| All samples[b] | 181 | 5.61 | 1.93 |
| Subswarm I | 26 | 5.52 | 1.50 |
| Subswarm II | 113 | 5.37 | 1.52 |
| Subswarm III | 42 | 6.33 | 2.92 |
| Subswarm IV[c] | 32 | 4.36 | 1.05 |

[a] Number of cores.
[b] Specimens from the subwarms 1 to III.
[c] Data from *Archanjo et al.* [2000].

expressed by $T = (\ln F - \ln L)/(\ln L + \ln F)$, where $L = k_1/k_2$ and $F = k_2/k_3$ [*Jelinek*, 1981]. $T = -1$ for a prolate or rod-shaped ellipsoid and $T = +1$ for an oblate or disc-shaped ellipsoid. Neutral or triaxial AMS ellipsoids have $T = 0$. The eccentricity of the ellipsoid, or degree of anisotropy, is shown by $P = k_1/k_3$ ranging from 1 (equal to sphere, isotropic) upward. The AMS data of the CMDS are presented in Table 1.

### 4.2. Low-Field Bulk Susceptibility and Anisotropy

[11] Bulk susceptibilities km (SI units) = 1/3 ($k_1 + k_2 + k_3$) of the CMDS are clustered in the range of 4.0 to 6.0 $\times$ $10^{-2}$ SI but extend from 2.0 to 12 $\times$ $10^{-2}$ SI. The average of all samples (5.61 $\times$ $10^{-2}$ SI) is close to the average of subswarms II and I and higher than the average of subswarm IV (Table 2). Subwarm III has the highest bulk susceptibility (6.33 $\times$ $10^{-2}$ SI, SD = 2.92), indicating a higher amount of ferrimagnetic grains compared with the others subswarms.

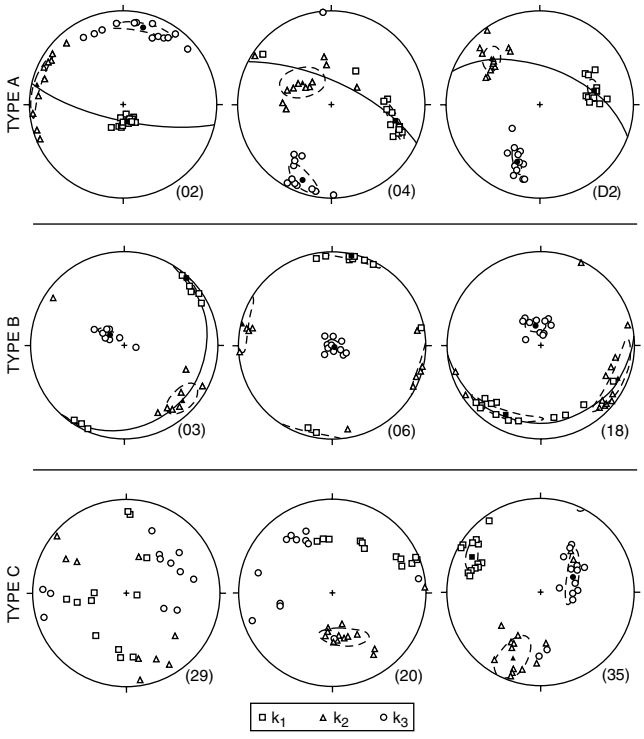


**Figure 4.** Equal-area projections (Schmidt net, lower hemisphere) of the AMS directional data (types A, B, and C) ($k_1$, maximum susceptibility or magnetic lineation; $k_2$, intermediate susceptibility; $k_3$, minimum susceptibility or pole of magnetic foliation). The dike plane is E-W, vertical, in all cases. Solid dots are the mean principal susceptibility directions, and the dashed lines represent their standard deviation (1$\sigma$). Solid line is the mean $k_1k_2$ plane.

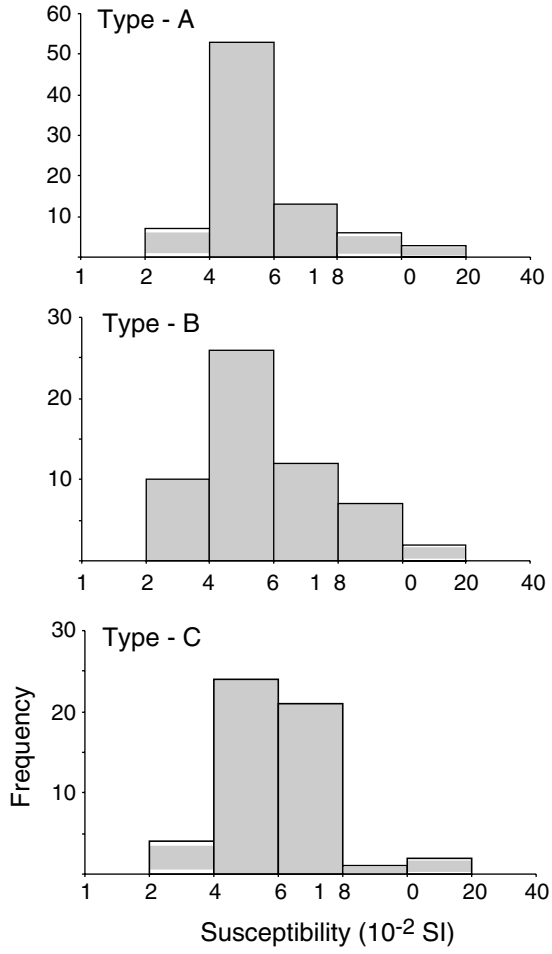


**Figure 5.** Histograms of the mean susceptibility values for the three types of AMS configurations.

[12] Rock magnetic studies showed that titanomagnetite is the main ferrimagnetic fraction of the basalt. Hysteresis properties revealed that the carriers of the magnetization are the finest grains with a pseudo-single-domain (PSD) structure with a trend toward multidomain (MD) behavior [*Bucker et al.*, 1986; *Archanjo et al.*, 2000]. Temperature dependence of the susceptibility showed Curie points in the range of 550°C and 575°C, indicating a practically titanium-free magnetite in agreement with the observation of ilmenite exsolution lamellae [*Bucker et al.*, 1986]. The drop of susceptibility on heating between 320°C and 450°C observed in various thermomagnetic curves attest to the presence of maghemite, indicating that the CMDS suffered a low-temperature oxidation event after the emplacement of the dikes.

[13] Despite the strong magnetic susceptibility of the CMDS, the degree of anisotropy is very low (mean of 1.020, SD = 0.014). As the low-field AMS of magnetite is due principally to its grain shape, the low degree of the bulk magnetic anisotropy mainly indicates a weak shape fabric of the ferrimagnetic grains.

### 4.3. Magnetic Fabric

[14] Three types of AMS configurations were observed in the mafic dikes (Figures 2 and 4). Type A has $k_3$ axes grouping

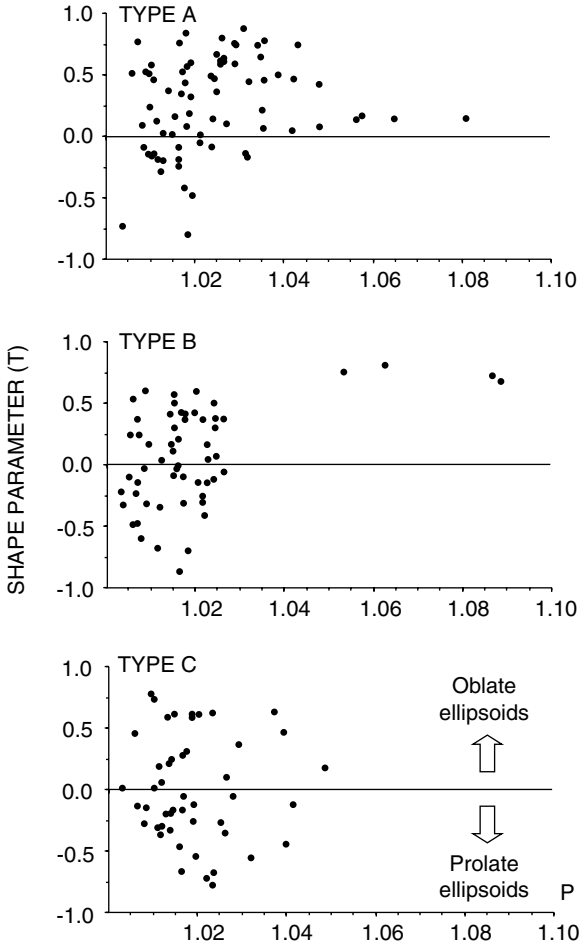


**Figure 6.** Shape parameter ($T$) of the AMS ellipsoid versus the degree of magnetic anisotropy ($P$) for the three types of AMS configurations.

nearly perpendicular to the dike plane. The magnetic lineation is generally subhorizontal, but locally, it may plunge steeply (Figure 4, dike 02). The foliation is usually subvertical and normally exhibits an angle lower than 35° from the plane of the dike. This kind of configuration, corresponding to a "normal" magnetic fabric, occurs at 42% of the sites. Type B fabric has $k_1$ axes clustering nearly perpendicular, or at a high angle, to the dike plane. The magnetic foliation usually dips gently, but locally, it may have steep dips trending almost perpendicular to the strike of the dike. This kind of configuration is termed "inverse" to very oblique and occurs at 34% of the sites. Type C fabric is scattered or uninterpretable. Generally, the principal directions of susceptibility are random, but in some dikes, $k_2$ axes are grouped (Figure 4, dike 20). Three dikes were included into this class showing the intermediate type of AMS fabric, i.e., $k_2$axes grouping almost perpendicular to the dike wall (Figure 4, dike 35). Type C fabric has bulk susceptibilities higher than types A and B (Figure 5) and its AMS ellipsoids occur in the oblate and prolate fields (Figure 6).

[15] Regionally the type A fabric shows a well-defined pattern (Figure 7). In four dikes around Lajes (subswarms II and III; dikes 1, 2, 28, and 14) the magnetic lineation plunges steeply. Far from Lajes the lineation plunges gently, except for one dike situated to the west of Angicos (dike 24) where the lineation is vertical. The same AMS pattern was observed to the south in subswarm IV, but there the subvertical lineations occur in the eastern part of the Santana Terrace [*Archanjo et al.*, 2000]. In the type A configuration the degree of anisotropy is generally lower than 1.04, and the AMS ellipsoids are dominantly of the oblate type (Figure 6). A highest degree of anisotropy ($P > 1.05$) was observed in dikes of subswarm III.

[16] Type B configuration occurs along the whole CMDS, principally in subswarms I and II (Figure 8). This kind of arrangement has magnetic lineations nearly perpendicular to the dike, the average strike of which is N-S. Regionally, the lineations trend north to NE in the eastern part of the swarm and to north to NW in the western part (see rose diagrams in Figure 8). The magnetic foliation usually has low to moderate dips. A variation of the type B configuration presents steep to moderate dipping foliations at a high angle to the dike plane

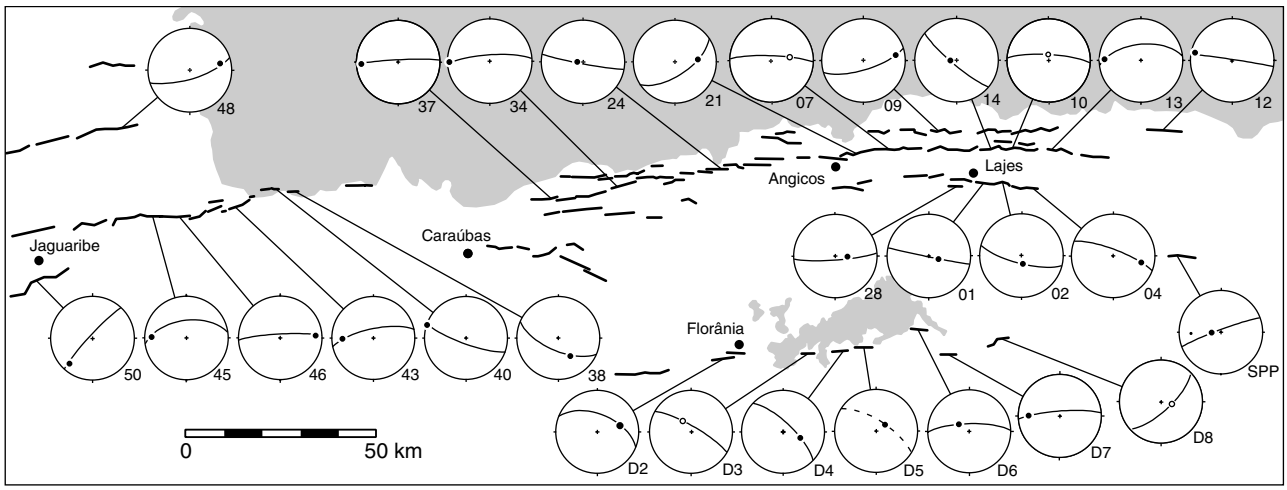


**Figure 7.** Mean site AMS principal directions of the type A (normal) magnetic fabric. Schmidt net, lower hemisphere; $k_1$, lineation (solid dot); $k_1k_2$ plane, foliation (solid line). Open dot and dashed line indicate ill-defined lineation and foliation, respectively. The AMS data from the subswarm IV (dikes D2 to D8) and dike SPP are from *Archanjo et al.* [2000].

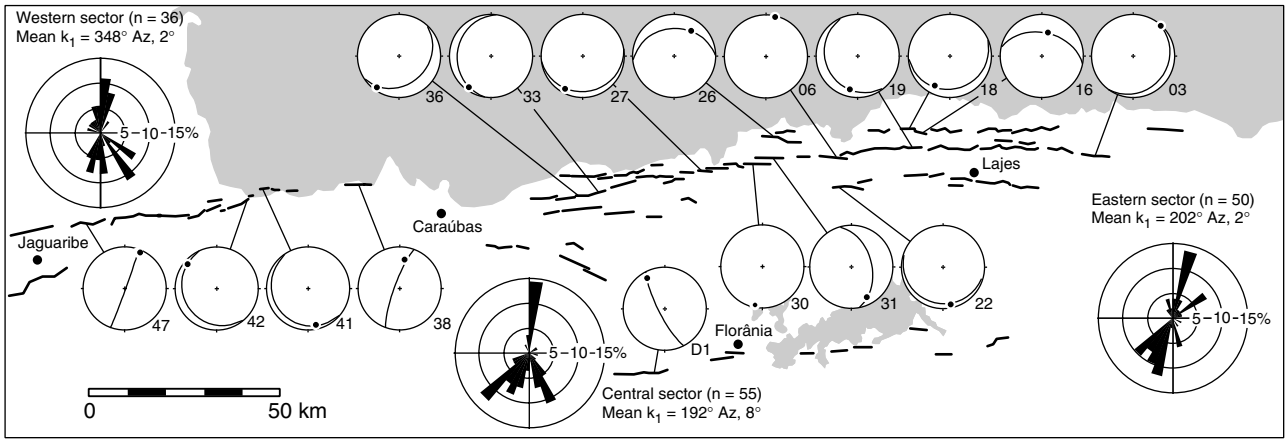


**Figure 8.** Mean site AMS principal directions of the type B (inverse to very oblique) magnetic fabric. The rose diagrams show the orientation of the magnetic lineations. Note that they vary from north to NE on the eastern segment of the swarm to north to NW on the western segment. Schmidt net, lower hemisphere; $k_1$, lineation (solid dot); $k_1k_2$ plane, foliation (solid line). The AMS data from the dike D1 (subswarm IV) are from *Archanjo et al.* [2000].

(dikes 38, 47, and D1). Both oblate to prolate AMS ellipsoids may occur in the type B fabric (Figure 6). The degree of anisotropy is typically lower than 1.03 but locally may increase up to 1.09.

## 5. Image Analysis and Bulk Mineral Subfabrics

[17] Fabrics in igneous rocks, when related to magmatic flow, result from statistical shape-preferred orientations (SPO) of rigid particles suspended in a viscous fluid. The SPO can be determined either from direct field measurements or from image analysis of sections/thin sections [*Shelley*, 1985; *Wada*, 1992; *Varga et al.*, 1998]. The magnitude and orientation of a given mineral fabric will depend on the shape of individual grains and on the degree of interaction between particles as crystallization proceeds [*Ildefonse et al.*, 1992]. Models using the suspension of particles freely rotating or concentrated enough to allow mechanical interactions have concluded that the SPO in magmatic rocks may be considered as indicating the local flow direction irrespective of the inferred flow mechanism [*Fernandez*, 1987; *Ildefonse et al.*, 1992].

[18] The SPO of plagioclase and opaque minerals from seven dikes of the Rio Ceará–Mirim swarm were studied in thin section by using the inertia tensor method [*Launeau and Cruden*, 1998]. The samples came from two dikes of subswarm III and one dike from subswarm IV corresponding to the type A magnetic fabric and from four dikes of subswarms I and II corresponding to the type B magnetic fabric. The AMS parameters of these samples are given in Table 3. From type A, one sample of subswarm III has a downdip magnetic lineation (dike 2), whereas in other cases the magnetic lineation plunges gently (dikes 4 and D2). The AMS ellipsoids are prolate and triaxial. The samples of subswarms I and II have $k_3$ axes grouping near the vertical. The $k_1$ axes are highly oblique (dikes 3, 18, and 27) or near perpendicular (dike 6) to the dike plane. The magnetic ellipsoids are triaxial to oblate.

### 5.1. Sample Preparation, Image Acquisition, and Analysis

[19] Standard thin sections were prepared from slabs cut parallel to the *xy*, *yz*, and *xz* frames of the cylindrical specimens used for the AMS study. This keeps independent the methods employed to calculate the ellipsoid of the inertia tensor and the principal directions of AMS. From each thin section, two high-resolution images were digitized through a rotating polarizer stage fixed to a microscope [*Fueten*, 1997]. This procedure yields $2^3$ image combinations for the determination of the inertia tensor ellipsoid of each specimen. Multispectral classification was used to identify opaque, plagioclase, clinopyroxene, and the fine-grained matrix on the basis of their color spectra [*Launeau et al.*, 1994]. This approach was not able to differentiate plagioclase and the fine-grained altered material because of their similar color. Thus, to separate the plagioclase, its twin planes were infilled with a specific color tone and subsequently detached from the fine-grained matrix by color identification. As many clinopyroxene grains were severely affected by hydrothermal alteration, this mineral population was discarded of the inertia tensor study. The classified modal fractions (percent) of opaque grains (1.0–6.2% Table 3) and plagioclase (14.6–27.8%) were calculated by dividing the number of pixels of each mineral class by the total number of pixels in the area of analysis.

[20] The classified images were used to calculate the inertia ellipse (two-dimensional (2-D)) of the opaque and plagioclase subfabrics for each *xy*, *yz*, and *xz* plane (Figure 9). The strength of each mineral phase is given by the shape ratio (SR) of the rose diagram of mean inertia ellipse after normalizing each classified object by its own surface. This prevents the shape effect of large grains on the inertia calculation. The orientation of each mineral fabric is given by the long axis of petrofabric ellipse measured with respect to *x*, *y*, and *z* axis of the thin section. The three mutually perpendicular $2 \times 2$ inertia tensors for each plane of analysis can be used to calculate $2 \times 2$ quadratic shape tensors, which can then be combined to calculate a $3 \times 3$ tensor and its corresponding ellipsoid [e.g., *Launeau and Cruden*, 1998]. This "inertia tensor ellipsoid" is characterized by a mean shape ratio (SR = $a/c$, where $a \geq b \geq c$ are the principal axis of the petrofabric) and orientation calculated from the average inertia tensor of the shapes. Finally, the orientation of the inertia tensor ellipsoid of each subfabric is rotated to geographic coordinates and then compared with the AMS ellipsoid.

### 5.2. Results

[21] Results are summarized in Table 3 and Figures 10, 11, and 12. The SR of opaque and plagioclase is usually several orders of magnitude greater than that of magnetic anisotropy of CDMS. The SR of plagioclase varies from 1.09 to 1.20, whereas that of opaque is normally lower than 1.11 but reaches 1.21 in

**Table 3.** Parameters of the Subfabrics of Opaque and Plagioclase Grains Calculated by the Inertia Tensor Method for the Dikes 2, 4 and D2 (Type A Magnetic Fabric) and Dikes 3, 6, 18, and 27 (Type B Magnetic Fabric) and Corresponding AMS[a]

| | ASM | | | | | Inertia Tensor | | | | | | | | | | | |
|---|---|---|---|---|---|---|---|---|---|---|---|---|---|---|---|---|---|
| | Km | $P$ | $T$ | $k_1$ | $k_3$ | Opaque | | | | | | Plagioclase | | | | | |
| | | | | | | $n$ | Percent | SR | $T$ | $a$ | $c$ | $n$ | Percent | SR | $T$ | $a$ | $c$ |
| | | | | | | | | | *Type A* | | | | | | | | |
| 02 | 7.79 | 1.02 | −0.43 | 182,71(1) | 031,17(3) | 108 | 5.0 | 1.05 | −0.44 | 193,65(8) | 001,26(18) | 180 | 20.5 | 1.10 | −0.02 | 227,68(15) | 356,15(30) |
| 04 | 10.94 | 1.02 | 0.07 | 114,28(5) | 207,6(3) | 132 | 6.0 | 1.08 | 0.54 | 246,21(24) | 352,32(8) | 183 | 19.3 | 1.11 | −0.11 | 186,73(21) | 330,16(28) |
| D2 | 5.59 | 1.04 | −0.21 | 082,40(3) | 205,31(5) | 117 | 6.2 | 1.08 | −0.20 | 032,18(18) | 297,16(34) | 148 | 16.5 | 1.12 | 0.38 | 050,32(32) | 147,10(14) |
| | | | | | | | | | *Type B* | | | | | | | | |
| 03 | 11.06 | 1.02 | −0.13 | 054,5(6) | 310,71(4) | 119 | 5.5 | 1.11 | 0.09 | 170,2(19) | 080,28(10) | 84 | 21.3 | 1.09 | 0.14 | 104,23(21) | 009,33(34) |
| 06 | 7.70 | 1.02 | 0.05 | 017,3(7) | 127,83(7) | 76 | 4.0 | 1.08 | −0.17 | 155,3(17) | 066,11(38) | 144 | 27.8 | 1.13 | 0.24 | 287,26(17) | 160,57(38) |
| 18 | 4.87 | 1.05 | 0.75 | 158,22(9) | 339,68(3) | 49 | 1.0 | 1.09 | 0.32 | 344,37(27) | 204,35(24) | 167 | 14.6 | 1.19 | 0.09 | 284,4(15) | 026,70(11) |
| 27 | 2.69 | 1.02 | 0.39 | 199,10(7) | 323,72(6) | 72 | 2.5 | 1.21 | −0.01 | 004,20(14) | 264,26(8) | 302 | 26.3 | 1.20 | 0.34 | 025,9(28) | 147,77(13) |

[a] The parameter $n$ is average of grains corresponding to sections $xy$, $xz$, and $yz$; percent is mean modal fraction corresponding the classified image of sections $xy$, $xz$, and $yz$; SR is shape ratio of the mineral fabric; Km is mean susceptibility ($10^{-2}$ SI); $P$ is degree of anisotrophy; $T$ is shape ellipsoid; $k_1$ and $k_3$ are the AMS mean directions (azimuth, plunge), and $a$ and $c$ are the mean directions of the shape ellipsoid and respective semiangle (in parentheses) of the ellipse of confidence around the means.

specimen 27. The opaque subfabric is, in addition, lower in type A than in type B (Table 3). The bulk $SR_{plag} > SR_{op}$ reflects the aspect ratio of the minerals that compose each population, formed by elongated laths of plagioclase and optically visible opaque grains of mainly cubic form. The mineral preferred orientation becomes best defined when SR is higher. No correlation is observed between the degree of magnetic anisotropy ($P$) and the petrofabric intensity (Figure 10). The shape ellipsoids of opaque subfabric vary from oblate to prolate, while the plagioclase is principally oblate. A poorly defined opaque fabric occurs in specimen 18, as shown by the wide semiangles of the cone of confidence ($1\sigma$) around the mean directions, which may be accounted to its unusual low modal abundance. Scattered $b$ and $c$ axes observed in opaque subfabric of specimens 6 and D2 are attributed to the linear configuration of the shape ellipsoid.

[22] Mineral shape fabrics are well-defined in the type A AMS configuration (Figure 11). For specimen 2 the subfabrics of opaque and plagioclase lies close to the direction of magnetic fabric. The foliation is almost parallel to the dike plane (E-W strike, vertical dip) and the lineation plunges downdip. The plagioclase subfabric of specimen 4 also plunges downdip, but the opaque lineation plunges shallowly. This discrepancy can be related to moderately oblate opaque subfabric ($T$ = 0.54) that makes reasonably close the pole of opaque foliation and $k_3$ and the mean $b$ axis of the subfabric and $k_1$ (Figure 11). In samples 4 and D2 the plagioclase foliation is oblique with respect to the dike plane, which may reflect imbrication of the silicate fabric. The orientation of plagioclase lineation of D2, however, is close to the magnetic lineation, although their shape ellipsoids are oblate and prolate, respectively, in this scale. The corresponding opaque subfabric is typically prolate, and the well-defined lineation makes a moderate (48°) angle to the mean $k_1$ axis.

[23] In the type B configuration the opaque preferred orientation is typically inverted with respect to dike orientation (Figure 12). The lineation lies at high angle to the confining wall, and when the fabric is well defined (samples 3 and 27), the foliation becomes perpendicular to the dike. This kind of configuration is found in magnetic fabric of four dikes of the CDMS (Figure 8; dikes 31, 38, 47, and D1). Dikes 3 and 27, however, display $k_3$ axes clustering near the vertical close to the mean $b$ axis of the opaque subfabric. A close correlation between a subhorizontal magnetic foliations and mineral fabric is observed in the plagioclase SPO of the specimens 6, 18, and 27. The plagioclase foliation is poorly defined in specimen 3 (semiangle of confidence is 34°), but its well-defined lineation, as well in specimens 6 and 18, plunges nearly parallel to the dike. For specimen 27 the opaque SPO is typically inverse. The fabric ellipsoid is triaxial ($T$ = −0.01) and oblate ($T$ = 0.34) for the plagioclase. The plagioclase lineation tends to form a girdle on the foliation that dips gently to the north. The mean opaque and plagioclase lineations, however, lie moderately close (23°) to each other. This mineral fabric, very similar to the type B configuration, indicates that (1) the inverse magnetic fabric of the dike 27 is not a grain size effect of ferrimagnetic particles and (2) that such an "atypical" mineral alignment within a vertical dike was formed in a magmatic stage, possibly by settling of crystals unrelated to flow.

## 6. Discussion

### 6.1. Origin of the Magnetic Susceptibility and Anisotropy

[24] The source of the low-field magnetic susceptibility of the Rio Ceará–Mirim dikes comes from the opaque grains. Plagioclase, the most important modal silicate of the dikes, has a negative susceptibility of the order of $-10^{-6}$ SI [*Tarling and Hrouda*, 1993]. Clinopyroxene has a positive susceptibility of

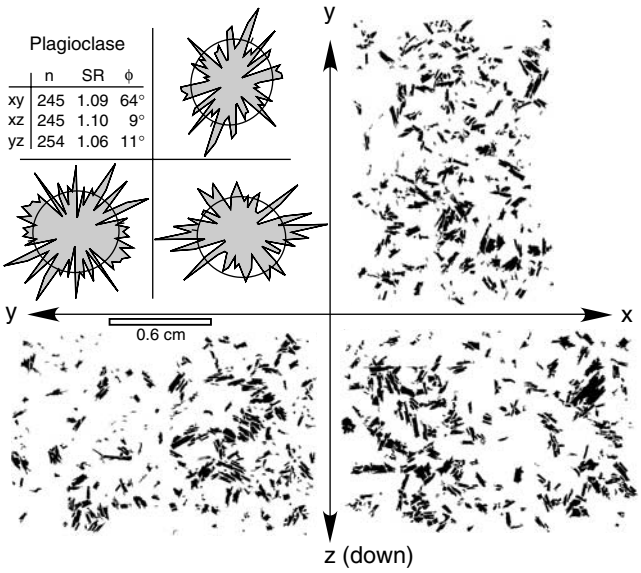


**Figure 9.** Distribution of plagioclase grains in three mutually perpendicular sections cut parallel to the reference axes *x*, *y*, and *z* (dike 18; subswarm I). The rose and the mean inertia tensor ellipse of each grain population are sketched in the top left. The parameters SR (shape ratio) and $\phi$ (angle between the long axis of the fabric and the reference axis, *x* or *y*) are used to calculate the quadratic shape tensor and 3-D ellipsoid (see Table 3 and Figures 11 and 12); *n* is number of objects.

$\sim 5 \times 10^{-4}$ SI, but its volume does not reach 15%, implying that its contribution to the bulk susceptibility must be minor. Hence the high bulk susceptibility of the dikes is given by a Ti-poor magnetite. The opaque grains of the basalts have a mean modal abundance of 4.8% and a mean grain size of the order of 100 μm. SEM examination show that the coarse oxide grains have cubic to needle-like shapes, and most of them exhibit incomplete faces in contact with the silicate matrix. The fine-grained oxides are found around the periphery of silicates or as a secondary product related to alteration of pyroxene and plagioclase. This secondary hydrothermal process may have formed maghemite, as observed in various thermomagnetic experiments, and carbonate found in the fine-grained matrix. The volumetrically dominant coarse-grained oxides must control the low-field susceptibility and anisotropy of the dikes, while the finest ferrimagnetic particles control the coercivity and remanence. Hysteresis data are interpreted in terms of PSD grains with a trend approaching MD field on a Day plot [*Bucker et al.*, 1986; *Archanjo et al.*, 2000].

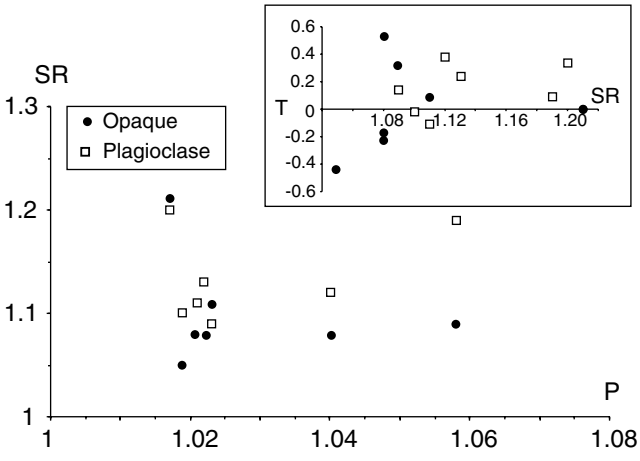


**Figure 10.** Results of image analysis of shape preferred orientation of opaque and plagioclase grains. The shape ratio (SR) of the fabric and the magnetic anisotropy (*P*) show no correlation. The shape ellipsoid of the plagioclase subfabric is principally oblate ($T > 0$), and its SR is normally higher than opaque subfabric (inset).

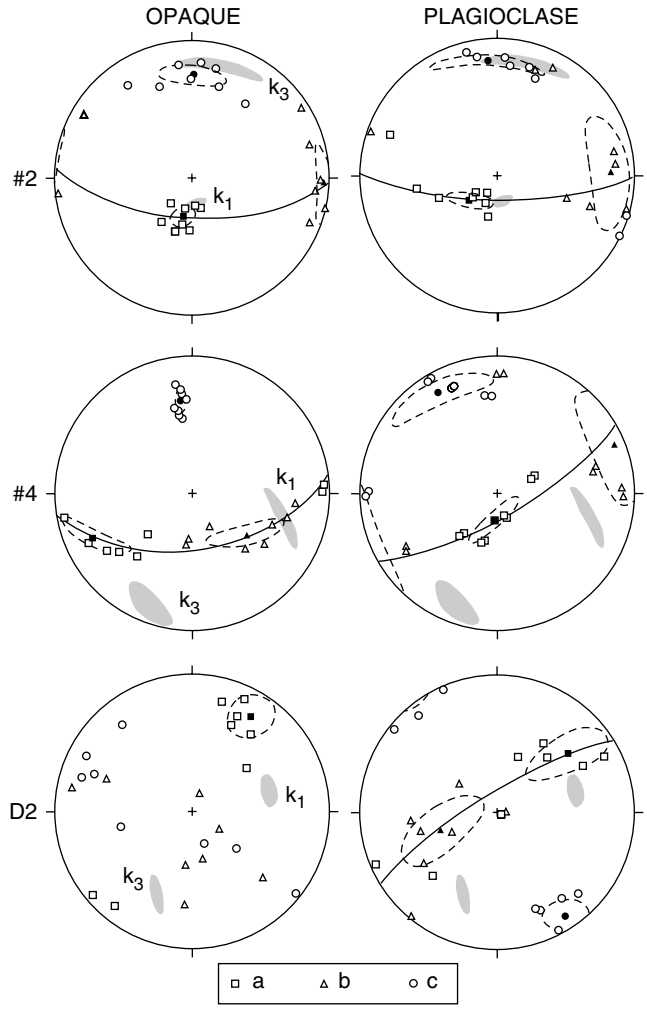


**Figure 11.** Shape-preferred orientation (subfabrics) of opaque and plagioclase of the type A magnetic fabric (dikes 2, 4, and D2). The shaded areas within each Schmidt net (lower hemisphere) are the ellipses of confidence of the AMS principal directions ($k_1$ and $k_3$); *a* (mineral lineation) $\geq$ *b* $\geq$ *c* (foliation pole) are the principal directions of the shape ellipsoid.

[25] In rocks with a magnetic susceptibility higher than $10^{-3}$ SI the AMS depends fundamentally on the shape-preferred orientation of ferrimagnetic particles [*Tarling and Hrouda*, 1993]. In igneous rocks it has been admitted that the preferred alignment of such particles is essentially controlled by the flow. The shape fabric of the opaque grains of type A magnetic fabric is consistent with a movement of magma within vertical dikes of E-W direction. This alignment of grains, however, would not be totally primary in origin because most oxides exhibit reaction textures with the silicate matrix as exemplified

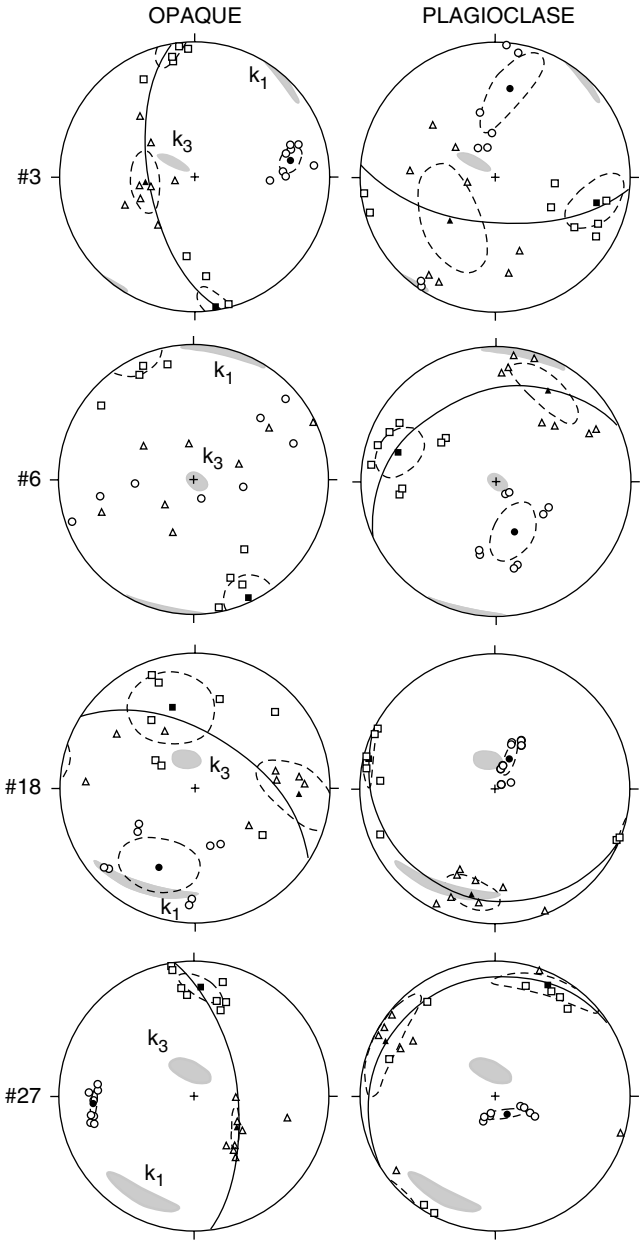


**Figure 12.** Shape-preferred orientation (subfabrics) of opaque and plagioclase of the type B magnetic fabric (dikes 3, 6, 18, and 27). The shaded areas within each Schmidt net (lower hemisphere) are the ellipses of confidence of the AMS principal directions ($k_1$ and $k_3$); $a$ (mineral lineation) $\geq b \geq c$ (foliation pole) are the principal directions of the shape ellipsoid.

by embayed contacts or round inclusions of silicate within the spinel. These textures, associated with ilmenite exsolution lamellae within magnetite [*Bucker et al.*, 1986], attest to the high-temperature oxidation event which accompanied cooling of these thick dikes.

### 6.2. Magnetic Fabric Pattern of the Rio Ceará–Mirim Swarm

[26] The two main configurations of the magnetic fabric, types A and B, are found all along the swarm usually without any preferred distribution, although type A is more common in subswarm IV (Figure 2). No particular relation was observed between dike width and fabric type; that is, type A, B, or C may be found along a single dike, as on the 150 ± 10 m wide dike situated NE of Jaguaribe (Figure 2).

**6.2.1. Type A magnetic fabric.** [27] In type A the AMS ellipsoids are usually oblate and the magnetic anisotropy is almost totally restricted between 1.01 and 1.04. The regional fabric pattern is relatively simple. The foliation in subswarms I, II, and III has a steep dip, and its strike is parallel to moderately oblique (<45°) to the dike wall. The lineations are mainly subhorizontal, except around Lajes, where in three dikes of subswarm III (1, 2, and 28) and one dike of subswarm II (14) they plunge downward. A vertical lineation is also observed at one site situated at west of Angicos (dike 24). However, this is only of local significance because the lineations observed in the nearest dikes have gentle to moderate plunges.

[28] The type A configuration has been reported as a normal magnetic fabric because it is compatible with a vertical dike. Assuming such a model, the flow system of the CMDS would have a fan-like geometry with a feeder zone around Lajes. A similar flow pattern has been suggested for subswarm IV [*Archanjo et al.*, 2000]. The shape fabric of plagioclase supports such an interpretation. Two dikes of subswarm III (2 and 4) have vertical lineations, and in three dikes (3, 6, and 18) far from Lajes, the lineations plunge gently (Figure 13). Plagioclase and opaque lineations have different orientations in dike 4, but the downdip, prolate-shaped plagioclase subfabric must record the vertical magma flow.

[29] To check the assumption that the downdip magnetic lineations of subswarm III would correspond to an upward flow, the imbrication of magnetic lineation of a vertical chilled margin [*Knight and Walker*, 1988] where the dike contacts are freshly exposed (dike 28, Figure 7) was investigated. The model assumes that the lineation of an uprising magma frozen against the wall rock must point upward in the direction of the dike plane [see *Tauxe et al.*, 1998, Figure 1]. The 1.2-m-wide dike cuts the foliation of host orthogneiss at a high angle. Thin, leucocratic aplite veins parallel to the gneissic foliation can be followed from one contact wall to the other with no apparent lateral offset, suggesting that the dilatation of the fracture, infilled by basaltic magma, occurred by N-S extension. Locally, the main dike branches into two parallel arms 0.8 m and 0.2 m wide. Cores were collected both at the chilled margin of the thickest dike at 1–2 cm from the contact wall as well as at the center of the dike. Both the northern and southern margins display well-clustered magnetic lineations that plunge at ~67°E (Figure 14). The mean magnetic foliation is parallel to the contact or shows a slightly obliquity (<10°) with it. The magnetic anisotropy of around 1.04 is higher than the anisotropy of the dike center ($P$ = 1.02). There, the obliquity of the magnetic foliation is higher than at the margins and the plunge of lineation is lower, ~52°E. The magnetic fabric of the chilled margins is consistent with a high inclination of magma fluxes. Since the imbrication angle of the magnetic lineation points inward, the chilled margin recorded downward flow, a feature that may occur in dikes following magma densification during crystallization. The phenomenon of magma backflow is not an unusual feature in igneous dikes [*Philpotts and Asher*, 1994], and it has been documented in volcanic centers apparently during the waning stages of an eruption [see *Rickwood*, 1990].

**6.2.2. Type B magnetic fabric.** [30] In the type B configuration, most $k_3$ axes have steep inclinations, and $k_1$ axes are generally perpendicular to the dike. Some dikes, principally those situated in the western part of subswarms II and IV, have $k_3$ axes grouping shallowly around the plane of the dike. The degree of anisotropy is usually lower than that of type A (1.005 < $P$ < 1.025), and the AMS ellipsoids vary from planar to linear. Such a fabric pattern may be found both in the center and near

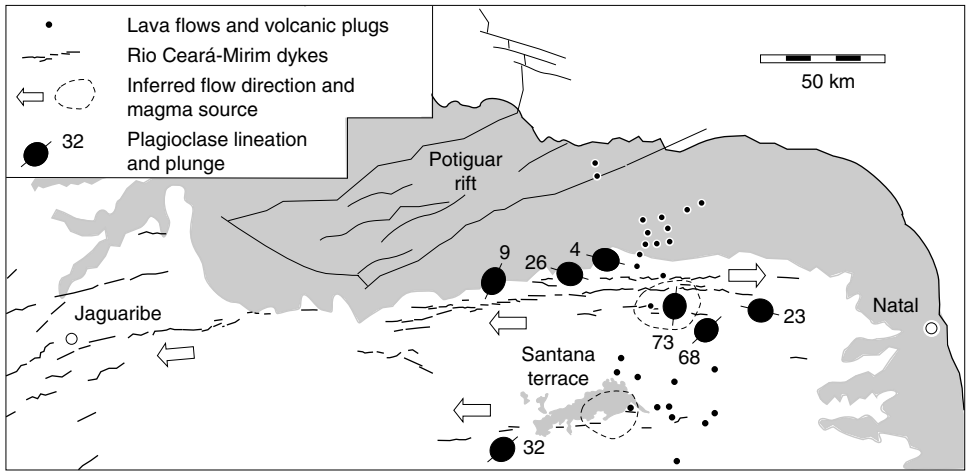


**Figure 13.** Inferred flow pattern of the Rio Ceará–Mirim Dike Swarm (arrows) and its presumed source area (dashed lines). Note that the supply of magma source may have occurred at the intersection with the Tertiary volcanic plugs. The ellipses correspond to the preferred orientation of the plagioclase lineation (in map view) and its respective plunge.

the margins of thick dikes, as verified in two dikes some 25 m wide situated west of Angicos (dike 30) and west of Caraúbas (dike 38) (Figure 14). Near the margin of dike 30 (0.20–1 m of the contact), the principal axes of susceptibility are well clustered with a mean horizontal lineation trending almost perpendicular to the dike wall. The foliation dips moderately to the west. The magnetic ellipsoid is slightly planar ($T = 0.18$), and the degree of anisotropy is low, around 1.02. In the dike center the ellipsoid is typically linear ($T = -0.78$). The degree of anisotropy is very low ($P = 1.01$), and as in the dike margin, the lineation occurs at high angle of the dike plane. The same low degree of anisotropy ($P = 1.01$) associated with a planar ellipsoid ($T = 0.30$) is found in the margin of dike 38 (0.8–1.5 m of the contact). The foliation dips steeply perpendicular to the dike plane. The lineations tend to be scattered in the foliation plane, but they preserve a moderate to shallow plunges in the N-S direction. Assuming that the infilling of these dikes occurred by E-W magma fluxes, the abnormal magnetic fabric found across the dike indicates that the type B configuration could have been acquired after magmatic flow had ceased.

[31] Study of the mineral fabric by image analysis revealed a good correlation between the orientation of the opaque lineation and $k_1$, except in dike 18 where $k_1$ and the long axis of the opaque subfabric are inverted. The magnetic foliation, on the other hand, is closer to the plagioclase foliation than that of the opaque foliation (Figure 12). The departure of $k_3$and the pole of the opaque foliation is attributed to the combined effect of the low shape ratio and ellipsoid symmetry of the opaque SPO. A low shape ratio would assist the exchange of the $a$ and $c$ axes of dike 18 and $b$ and $c$ axes of dikes 3 and 27 that show oblate and triaxial to prolate symmetry, respectively. The similarities between some type C configurations (dikes 20 and 35, Figure 4) with the plagioclase subfabric (specimen 18, Figure 12) also support these assumptions. An intermediate AMS configuration ($k_2$ is the pole of the dike) could be easily formed by flipping the $b$ (= $k_2$) and $c$ (= $k_3$) axes of a triaxial to prolate opaque subfabric that rests on a template of gently dipping plagioclase laths. A typical type B configuration may also be formed by flipping $k_2$ and $k_3$, while the magnetic lineation occurs at high angle to the dike plane. Hence no SD particle effect or distribution anisotropy of magnetic oxides is necessary to explain the abnormal AMS fabric of the CMDS. Instead, the highly oblique to inverse magnetic fabrics have their

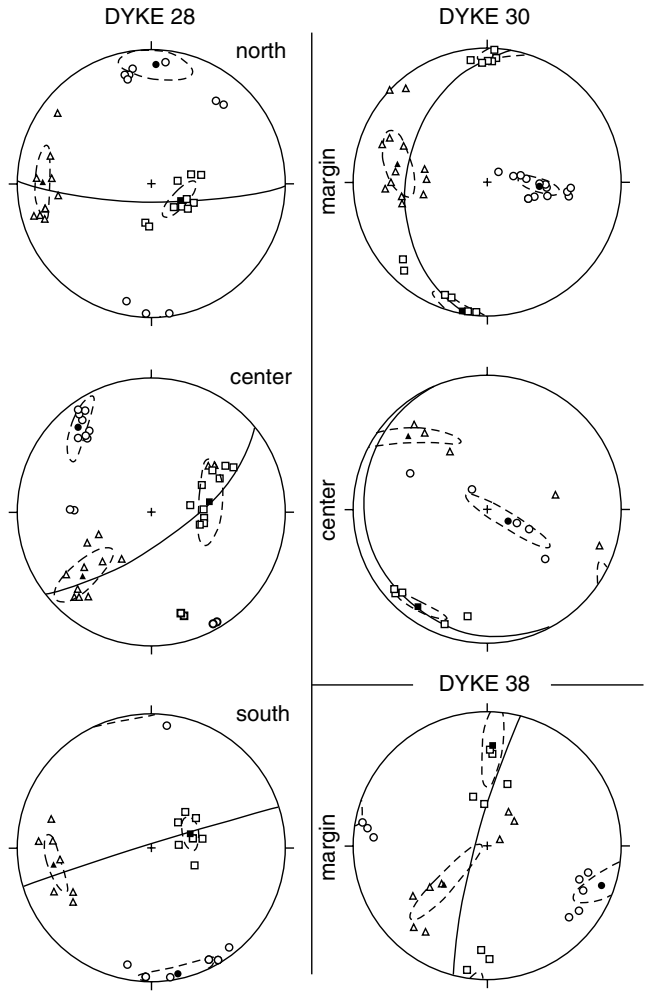


**Figure 14.** Magnetic fabric of the chilled margins of the dike 28 (see localization on Figure 7) and center and margin of dike 30 and margin of dike 38 (see localization on Figure 8). The symbols are as shown in Figure 4.

origin in the SPO of coarse opaque grains. On the basis of these observations, two different models are proposed to account for the magnetic fabric development.

1. The magnetic fabric would be formed along with magmatic flow. The origin of type B fabric could be due to rolling of elongated particles [*Jeffery*, 1922] and/or to free rotation of particles in a viscous magma, which would lead to abnormal fabric types, following the *Dragoni et al.* [1997] model. The postemplacement high-temperature reactions that affected the magnetic oxides would not be able to erase the primary abnormal fabric. The static high-temperature recrystallization of Ti-poor magnetite would lower the bulk anisotropy, and in a more advanced stage, the magnetic fabric would be randomized.

2. The type B magnetic fabric would be unrelated to magmatic flow. In this model the crystallization of magnetite would occur within the residual magma volumes remaining after the earlier silicates had crystallized. Following *Launeau and Cruden* [1998], drag and collision within a crystal-enriched magma would result in the creation of opening and closing directions controlled by the stretch of the magma. As crystallization proceeds, late crystallizing interstitial magnetite would be forced to grow into spaces whose shape depends on the silicate framework [see *Launeau and Cruden*, 1998, Figure 12]. By the time the magma locks completely, these grains would tend to be aligned both along the plagioclase lineation and perpendicular to it. Inverse fabric would occur when oxide grains aligned perpendicular to the plagioclase lineation overcome the oxide grains aligned in the flow direction: the bulk anisotropy of the magnetic fabric, consequently, tends to decrease.

[32] Model 2 fits better to our data because it takes in account the silicate framework in the AMS development. The subfabrics of opaque and plagioclase of the dike 27 (Figure 12) illustrate this point. The origin of the oblate plagioclase subfabric ($T = 0.34$) is attributed to a late stage settling of crystals or to sinking of a dense mush in a stationary magma volume. Vertical compaction would rearrange any earlier magmatic structure by scattering the plagioclase lineation on a subhorizontal foliation. The shape ratio of the opaque subfabric would increase because of interstitial growth within the silicate framework and/or grain rotations into the stretching direction of the magma. A well-defined opaque (and magnetic) lineation perpendicular to the dike wall indicates that the late stage magma stretching was close to the extension direction of the regional paleostress field. Complex or uninterpretable AMS configurations are predicted if, for example, the bulk fabric is formed by the intersection of two or more incompletely erased subfabrics with different symmetries and magnitudes.

### 6.3. Regional Implications

[33] The regional pattern of magnetic structures that emerges from the CMDS is of a horizontal movement of magma within dikes with a supply area probably situated around Lajes. Lateral flow is not an unusual feature in dike swarms as observed in a variety of studies from major eruptive events in Iceland and Hawaii [*Sigurdsson*, 1987; *Wilson and Head*, 1988]. The lateral movement of the magma must be greater than the vertical movement, a condition that is satisfied when the magma density is equal to the density of the surrounding regional host rock [*Ryan*, 1987]. In most cases such upflow regions are situated at shallow depths beneath central volcanoes. In the CMDS this ''source zone'' would have occurred at the intersection of volcanic necks and lava flows of Tertiary age (Figure 13). The same relationship was observed in subswarm IV, but there the feeder zone may have been situated under the eastern part of fluvial sandstones of the Santana Terrace. Either these patterns can be regarded as fortuitous, or another explanation must be sought. A tentative model for this latter alternative relates to the presence of Early Cretaceous volcanic centers occupied in the Tertiary by volcanic plugs. They could have shared the same mantle reservoirs, with the tholeiitic magma that fed the dikes evolving to an alkaline magmatism in the Tertiary by the deepening of mantle sources as the South American plate drifted westward.

## 7. Conclusion

[34] Shape-preferred orientation of both opaque grains and plagioclase laths keep a close relation with the two main magnetic fabric types found in the CMDS. The normal AMS type provides a good image of the movement of the magma within the dikes. Regionally, it is characterized by lateral magma fluxes in the 350-km-long swarm, except at its intersection with the Tertiary volcanic plugs where the flow becomes subvertical. There, the downdip magnetic lineation matches with the vertical lineation of plagioclase laths, suggesting that the supply of magma may have been situated around Lajes. Backflow processes, however, were found in the pattern of chilled lineations measured on both margins of a single dike. In addition, exchange of $k_1$ and $k_2$ or $k_2$ and $k_3$ may occur in oblate or prolate fabrics even with moderate shape factor ($-0.5 > T > 0.5$). These findings indicate that interpretation of AMS in terms of flow kinematics for the more eccentric fabrics must taken with caution and that key domains, like possible feeder zones, should be confirmed by examining the petrofabric. Some dikes, however, display mineral fabrics that are incompatible with flow within a vertical confining walls. Settling of crystal and/or vertical compaction of the magma column in long-lived thick dikes would be able to form a planar plagioclase shape fabric, which could be used as a template for developing a subhorizontal magnetic foliation found in some dikes

[35] The opaque shape ellipsoid also agrees well with the highly oblique to inverse AMS principal directions. Opaque and magnetic lineations are found roughly perpendicular to the plagioclase lineation, the latter normally aligned along the dike. Abnormal AMS types are attributed to crystallization of magnetic oxides in residual magma volumes accommodated into spaces opened normal to the stretching direction. A high-temperature oxidation stage on cooling of the dikes recrystallizes a nearly pure magnetite, which could locally grow following the regional stress field.

[36] A third AMS configuration is related to random distribution of principal susceptibility axes, or fabric types that cannot be interpreted. Some random fabrics occur in hydrothermally altered dikes, which may have disorganized any grain alignment. Incomplete recrystallization of magnetic oxides, associated with intersection of subfabrics, may have resulted in the complex fabric types observed in the CMDS.

[37] **Acknowledgments.** This project was supported by grants from Fundaç ão de Amparo a Pesquisa do Estado de São Paulo (FAPESP, 98/04420-2 and 98/13250-3) and Conselho Nacional de Desenvolvimento Científico e Tecnológico (CNPq), to which we are thankful. We are also grateful to M. I. B. Raposo for help with the AMS measurements. Constructive reviews by Bernie Housen and an anonymous reviewer helped to improve the manuscript.

## References

Archanjo, C. J., R. I. F. Trindade, J. W. P. Macedo, and M. G. Araújo, Magnetic fabric of a basaltic dyke swarm associated with Mesozoic rifting in northeast Brazil, *J. South Am. Earth Sci.*, *13*, 179–189, 2000.

Bellieni, G., Evidence of magmatic activity related to Middle Jurassic and Lower Cretaceous rifting from northeastern Brazil (Ceará–Mirim): K/Ar age, paleomagnetism, petrology and Sr-Nd isotope characteristics, *Chem. Geol.*, *97*, 9–32, 1992.

Bucker, C., A. Schult, W. Bloch, and S. D. C. Guerreiro, Rock magnetism and paleomagnetism of an Early Cretaceous/Late Jurassic dyke swarm in Rio Grande do Nortem, Brazil, *J. Geophys.*, *60*, 129–135, 1986.

Dragoni, M., R. Lanza, and A. Tallarico, Magnetic anisotropy produced by magma flow: Theoretical model and experimental data from Ferrar dolerite sills (Antarctica), *Geophys. J. Int.*, *128*, 230–240, 1997.

Elwood, B. B., Flow and emplacement direction determined for selected basaltic bodies using magnetic susceptibility anisotropy measurements, *Earth Planet. Sci. Lett.*, *41*, 254–264, 1978.

Ernst, R. E., Magma flow directions in two mafic Proterozoic dyke swarms of the Canadian Shield as estimated using anisotropy of magnetic susceptibility data, in *Mafic Dykes and Emplacement Mechanisms*, edited by A. J. Parker, P. C. Rickwood, and D. H. Tucker, pp. 231–235, A. A. Balkema, Brookfield, Vt., 1990.

Ernst, R. E., and W. R. A. Baragar, Evidence from magnetic fabric for the flow pattern of the magma in the Mackenzie giant radiating dyke swarm, *Nature*, *356*, 511–513, 1992.

Fernandez, A., Preferred orientation developed by rigid markers in two-dimensional simple shear strain: A theoretical and experimental study, *Tectonophysics*, *136*, 151–158, 1987.

Fialko, Y. A., and A. M. Rubin, Thermal and mechanical aspects of magma emplacement in giant dike swarms, *J. Geophys. Res.*, *104*, 23,033–23,049, 1999.

Fueten, F., A computer controlled rotating polarizer stage for the petrographic microscope, *Comput. Geosci.*, *23*, 203–208, 1997.

Ildefonse, B. P., P. Launeau, J. L. Bouchez, and A. Fernandez, Effect of mechanical interaction on the development of shape preferred orientations: A two-dimensional experimental approach, *J. Struct. Geol.*, *14*, 73–83, 1992.

Jeffery, G., The motion of ellipsoidal particles immersed in a viscous fluid, *Proc. R. Soc. London, Ser. A*, *102*, 161–179, 1922.

Jelinek, V., Characterization of the magnetic fabrics of rocks, *Tectonophysics*, *79*, T63–T67, 1981.

Knight, M. D., and G. P. L. Walker, Magma flow directions in dikes of the Koolau Complex, Oahu, determined from magnetic fabric studies, *J. Geophys. Res.*, *93*, 4301–4319, 1988.

Launeau, P., and A. R. Cruden, Magmatic fabric acquisition mechanisms in a syenite: Results of a combined anisotropy of magnetic susceptibility and image analysis study, *J. Geophys. Res.*, *103*, 5067–5089, 1998.

Launeau, P., A. Cruden, and J. L. Bouchez, Mineral recognition in digital images of rocks: A new approach using multichannel classification, *Can. Mineral.*, *32*, 919–933, 1994.

Maluski, H., C. Coulon, M. Popoff, and P. Baudin, $^{40}Ar/^{39}Ar$ chronology, petrology and geodynamic setting of Mesozoic to early Cenozoic magmatism from the Benue Trough, Nigeria, *J. Geol. Soc. London*, *152*, 311–326, 1995.

Matos, R. M. D., The northeast Brazilian rift system, *Tectonics*, *11*, 766–791, 1992.

Morgan, J. W., Hotspot tracks and the early rifting of the Atlantic, *Tectonophysics*, *94*, 123–139, 1983.

O'Connor, J. M., and A. P. Le Roex, South Atlantic hot spot plume systems: Distribution of volcanism in time and space, *Earth Planet. Sci. Lett.*, *113*, 343–364, 1992.

Oliveira, D. C., O papel do Enxame de Diques Rio Ceará–Mirim na evolução tectônica do Nordeste Oriental (Brasil): Implicações na formação do Rifte Potiguar, Ms.C. thesis, Univ. Fed. de Ouro Preto, Ouro Preto, Brazil, 1992

Park, J. K., E. I. Tanczyk, and A. Desbarats, Magnetic fabric and its significance in the 1400 Ma Mealy diabase dikes of Labrador, Canada, *J. Geophys. Res.*, *93*, 13,689–13,704, 1988.

Philpotts, A. R., and P. M. Asher, Magmatic flow-direction indicators in a giant diabase feeder dike, Connecticut, *Geology*, *22*, 363–366, 1994.

Raposo, M. I. B., and M. Ernesto, Anisotropy of magnetic susceptibility in the Ponta Grossa dike swarm (Brasil) and its relationship with magma flow directions, *Phys. Earth Planet. Inter.*, *87*, 183–196, 1995.

Rickwood, P. C., The anatomy of a dyke and the determination of propagation and magma flow directions, in *Mafic Dykes and Emplacement Mechanisms*, edited by A. J. Parker, P. C. Rickwood, and D. H. Tucker, pp. 81–100, A. A. Balkema, Brookfield, Vt., 1990.

Rochette, P., L. Jenatton, C. Dupuy, F. Boudier, and I. Reuber, Diabase dikes emplacement in the Oman ophiolite: A magnetic fabric study with reference to geochemistry, in *Ophiolite Genesis and Evolution of the Oceanic Lithosphere*, edited by T. Peters, A. Nicolas, and R. G. Coleman, pp. 55–82, Kluwer Acad., Norwell, Mass., 1991.

Rochette, P., M. Jackson, and C. Aubourg, Rock magnetism and the interpretation of anisotropy of magnetic susceptibility, *Rev. Geophys.*, *30*, 209–226, 1992.

Rochette, P., C. Aubourg, and M. Perrin, Is this magnetic fabric normal? A review and case studies in volcanics formations, *Tectonophysics*, *307*, 219–234, 1999.

Ryan, M. P., Neutral buoyancy and mechanical evolution of magmatic systems, in *Magmatic Processes: Physiochemical Principles*, edited by B. O. Mysen, *Geochem. Soc. Spec. Publ., 1*, 259–287, 1987.

Shelley, D., Determining paleo-flow directions in dykes from groundmass fabrics in the Lyttelton radial dykes, New Zealand, *J. Volcanol. Geotherm. Res.*, *25*, 69–79, 1985.

Sial, A. N., L. E. Long, D. A. R. Pessoa, and K. Kawashita, Potassium-argon ages and strontium isotope geochemistry of Mesozoic and Tertiary basaltic rocks, northeastern Brazil, *An. Acad. Bras. Cienc.*, *53*, 115–122, 1981.

Sigurdsson, H., Dyke injection in Iceland: A review, in *Mafic Dyke Swarms*, edited by H. C. Halls and W. F. Fahrig, pp. 55–64, Geol. Assoc. of Can., Vancouver, B. C., 1987.

Stephenson, A., S. Sadikun, and D. K. Potter, A theoretical and experimental comparison of the anisotropies of magnetic susceptibility and remanence in rocks and minerals, *Geophys. J. R. Astron. Soc.*, *84*, 185–200, 1986.

Tarling, D. H., and F. Hrouda, *The Magnetic Anisotropy of Rocks*, 217 pp., Chapman and Hall, New York, 1993.

Tauxe, L., J. S. Gee, and H. Staudigel, Flow directions in dikes from anisotropy of magnetic susceptibility data: the bootstrap way, *J. Geophys. Res.*, *103*, 17,775–17,790, 1998.

Varga, R. J., J. S. Gee, H. Staudigel, and L. Tauxe, Dike surface lineation as magma flow indicators within the sheeted dike complex of the Troodos Ophiolite, Cyprus, *J. Geophys. Res.*, *103*, 5241–5256, 1998.

Wada, Y., Magma flow directions inferred from preferred orientations of phenocryst in a composite feeder dike, Miyake-Jima, Japan, *J. Volcanol. Geotherm. Res.*, *49*, 119–126, 1992.

Wilson, L., and J. H. Head, Nature of local magma storage zones and geometry of conduit systems below basaltic eruptions sites: Pu'u O'o Kilauea East Rift, Hawaii, *J. Geophys. Res.*, *93*, 14,785–14,792, 1988.

M. G. S. Araújo, Programa de Pós-Graduação em Geoquímica e Geotectônica, Instituto de Geociências, rua do Lago 562, São Paulo, SP, 05508-900 Brasil. (marcelus@usp.br)

C. J. Archanjo, Universidade de São Paulo, Instituto de Geociências, rua do Lago 562, São Paulo, SP, 05508-900 Brasil. (archan@usp.br)

P. Launeau, Laboratoire de Planétologie et Géodynamique, Faculté de Sciences et des Techniques, Université de Nantes, 2 rue de la Houssinière, Nantes 44322, France. (launeau@chimie.univ-nantes.fr)